



## **DE-BONDED DIAGONALLY REINFORCED BEAM FOR GOOD REPAIRABILITY**

**Kazushi Shimazaki<sup>1</sup>**

### **SUMMARY**

Good repairability is required to enable the reuse of buildings after severe earthquakes, even for RC members. A beam with diagonal reinforcements is very ductile. However, when the diagonal reinforcements yield under tension, tension stress is applied to the concrete along the entire length by bond stress. This increases the number of concrete cracks. De-bonded diagonal reinforcements and a small design of narrow U-shaped notches near the end of the beam are one solution to reduce damage and increase the ability to absorb energy. The experimental results showed an effective means to reduce damage with greater energy dissipation ability.

### **INTRODUCTION**

The goal of the earthquake resistant design of any country is to protect life in very severe earthquakes by providing for buildings with strength and durability to resist collapse. After a severe earthquake such as the Great Hanshin Earthquake, however, the demands of building owners changed: they want to be able to use the buildings again, with small repair cost. This requires good repairability even for RC members.

For reinforced concrete buildings with a “shear core”, short beams are connected to the shear walls as shown in Figure 1. To satisfy the ductility demand of the beams, diagonal reinforcements have been used [1]. Many experimental studies were carried out on using diagonal reinforced beams as members of a tube structure [e.g. 2, 3]. Although these beams showed very ductile behavior, the number of concrete cracks was quite large and damage to the beams prevented repair work. In those beams, the diagonal reinforcements yielded on the tension side only because concrete struts work with them on the compression side. This increases the number of concrete cracks, and increases the beam length. Repair work is thus laborious.

The working stress of diagonal reinforcements is constant with respect to the overall length, so there is no need for bond stress between the diagonal reinforcements and concrete. De-bonded diagonal reinforcements are one solution to reduce the number of concrete cracks. A small design at the end of the beam can make the diagonal reinforcements yield on the compression side. It also reduces tension stress of

---

<sup>1</sup> Kanagawa University, JAPAN Email: shimak19@kanagawa-u.ac.jp

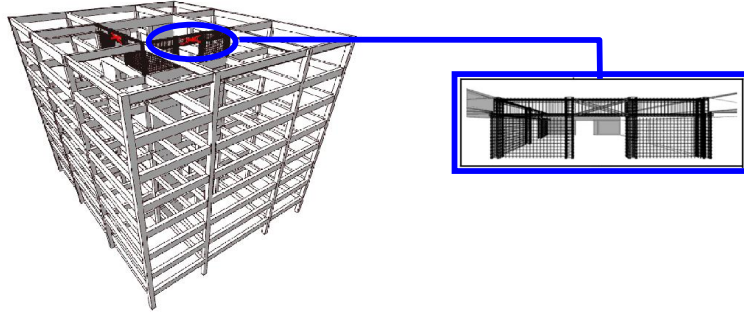


**Figure 1:** Short beams in a reinforced concrete buildings with shear core

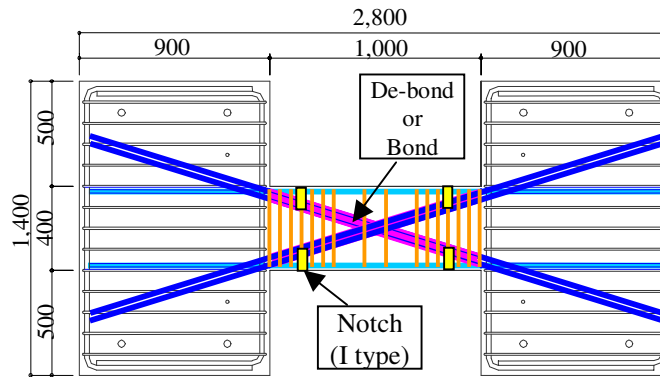
concrete caused by Poisson's effect from compression stress. This means that the ability to absorb energy will increase and the number of concrete cracks will not increase.

This paper presents an outline of a study on short beams with diagonal reinforcements to reduce concrete cracks and thus improve repairability, by providing greater energy dissipation ability.

## EXPERIMENTAL PROGRAM

### Test specimens

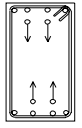
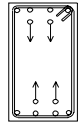
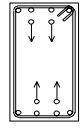
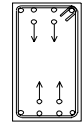
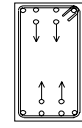
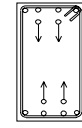
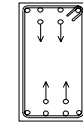
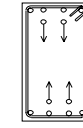
The dimensions of the specimens are shown in Figure 2. All beams had eight diagonal reinforcement bars with four longitudinal reinforcement bars and web reinforcements. The section is 200 mm thick, 400 mm high and 1000 mm long. The overall length of the specimen is 2800 mm with end stubs 400 mm thick, 1400 mm high and 900 mm long at both ends. These dimensions are one-third scale of the prototype structure shown in Figure 1.



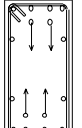
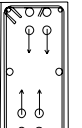
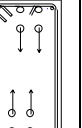
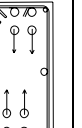
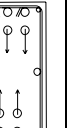

**Figure 2:** Dimensions of Test Specimens

The specimens are divided into two series, one nominal and the other progressive. The first of the series is summarized in Table 1. The primary experimental parameter is the bond of diagonal reinforcements, the second is the amount of web reinforcement, and the third is the strength ratio of rebar and concrete. Specimens #N-1 and #N-2 are common diagonal reinforcement beams, and specimens #N-3 to #N-8 are beams with de-bonded diagonal reinforcements. The amount of web reinforcement provided for #N-1 and #N-3 is consistent with the current AIJ standard [4, experimental equation]. For #N-2 and #N-4, the amount is calculated according to the AIJ design guidelines [5, truss model equation] with  $R = 1/50$  inelastic rotational ability. For #N-5, 6, 7 and 8, the amount at both end parts is doubled. The concrete compressive strength and the yield stress of the reinforcements are summarized in Table 1.

**Table 1 : List of the first series' specimens**

Specimen	No.N-1	No. N-2	No. N-3	No. N-4	No. N-5	No. N-6	No. N-7	No. N-8	
Section									
b×D(mm)	200×400								
Concrete (N/mm <sup>2</sup> )	54	51	54	51	51	64	48	32	
Parallel bars	Bars	2-D16							
	σ <sub>y</sub> (N/mm <sup>2</sup> )	476	459	476	459		432	456	
X Shape bars	Bars	4-D16 Bond		4-D16 De-bond			4- ϕ 16 De-bond	4- ϕ 19 De-bond	4- ϕ 16 De-bond
	σ <sub>y</sub> (N/mm <sup>2</sup> )	476	459	476	459		386	380	383
Web bars	Bars	2-D6 @ 150	2-D6 @ 100	2-D6 @ 150	2-D6 @ 100	2-D6 @ 100/@ 50			
	σ <sub>y</sub> (N/mm <sup>2</sup> )	331	337	331	337		308	349	
	p <sub>w</sub> (%)	0.21	0.32	0.21	0.32	0.32/0.64			
Tested year	2000	2001	2000	2001		2002	2003		

**Table 2 : List of the I series' specimens**

Specimen		No.I-1	No. I-2	No. I-3	No. I-4	No. I-5	No. I-6
Section							
b×D(mm)		200×400					
Concrete(N/mm <sup>2</sup> )		54	64	64	49	33	33
Parallel bars	Bars	2-D16	2-D10				
	σ <sub>v</sub> (N/mm <sup>2</sup> )	476	370		380		
Axial bars	Bars	4-D16 Bond	2-D16 Bond	-	2- ϕ 19 De-bond		-
	σ <sub>v</sub> (N/mm <sup>2</sup> )	476	849		380		
X Shape	Bars	4-D16 Bond	4- ϕ 19 De-bond				
	σ <sub>v</sub> (N/mm <sup>2</sup> )	476	386		380		
Web	Bars	2-D6 @ 150	2-D6 @ 100/@50				
	σ <sub>y</sub> (N/mm <sup>2</sup> )	331	308		349		
	p <sub>w</sub> (%)	0.21	0.32/0.64				
Tested year		2000	2002		2003		

The other series (I series) is summarized in Table 2. These are improved ones having small notches near the beam end to reduce concrete cracks and thus improve repairability. Specimen #I-1 has 4-D16 parallel reinforcements anchored into the stub and the others have 2-D10 parallel reinforcements without anchoring into the stub. The notches are at the beam-end for specimen #I-1, and at 150 mm inside from the beam-end for specimens #I-2 through 6. All diagonal reinforcements are de-bonded. The amount of

web reinforcement of #I-1 is the same as in #N-1 and 3, and the others are the same as in #N-5 to 8. The concrete compressive strength and the yield stress of the reinforcements are summarized in Table 2. Specimens #I-1, 2, 4, and 5 have axial reinforcements to deduce axial elongation. #I-1 and 2 are with bond and #I-4 and 5 are without.

### De-bonded reinforcement

To create de-bonded reinforcement bars, wax and de-bond material (butylene rubber) were used for the deformed bars. First, the dimple parts of the deformed bar were filled with wax, and the bar was coated with de-bond material (butylene rubber), and then covered by gummed tape. The anchor part (the part in the stub) was untouched. For a round bar, to anchor into the stub part, deformed bars were welded at both sides as shown in Figure 3(b). The round bar was coated with de-bond material (butylene rubber), and then covered by gummed tape, the same as with the deformed bars.

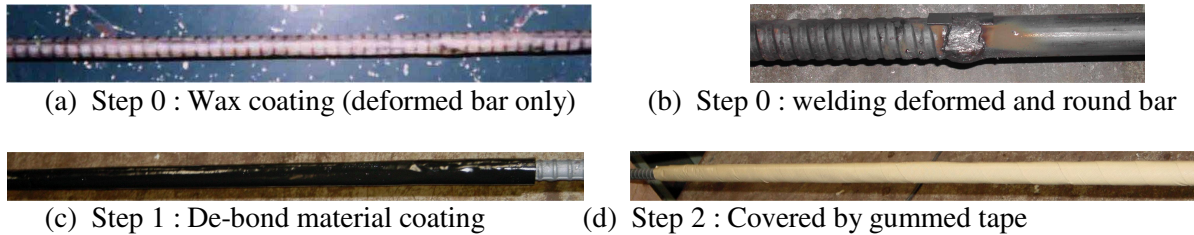


**Figure 3 : De-bonded reinforcement bar**

### Test setup

The bottom of the specimen rotated 90° was bolted to the loading frame. An L-shaped loading beam 500 mm wide by 600 mm deep was placed on top of the specimen, and a main hydraulic actuator was attached at mid-height of the beam. Two sub hydraulic actuators were attached at the top to control the level of loading beam as shown in Figure 4. Antisymmetric bending moment was applied to the specimen.

### Loading cycles

Loading cycles as shown in Figure 5 were applied to increase drift angle  $R$  with 3 repeated cycles. Only at the level of  $R = 1/100$  was the loading cycle conducted with 6 repeated cycles. These were determined by dynamic response analysis for the prototype building shown in Figure 1 during a severe earthquake to satisfy the energy dissipation ability. Specimens #6 and #8 were repaired after at the level of the  $R = 1/100$  cycle for #6, and  $1/67$  for #8. Then they were reloaded from the level of  $R = 1/200$ .

### Instrumentation

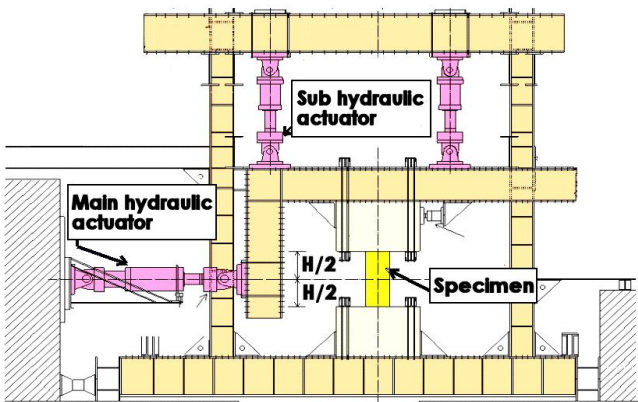


**Figure 4 : Test Setup**

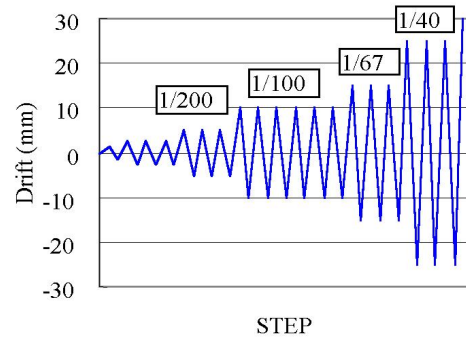


**Figure 5 : Loading Cycles**

During the tests, total drift was measured as the displacement difference of the loading stubs. Partitioned axial displacements to calculate bending deformation were measured at both flanges as shown in Figure 6. Shear deformation was calculated by subtracting the calculated bending deformation from the measured total deformation. Strains of the reinforcements were also measured by strain gauges mounted at several locations along diagonal reinforcements, longitudinal reinforcements and on the transverse bars.

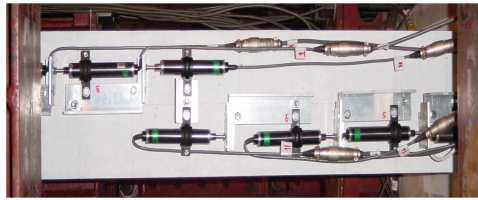


**Figure 6 :** Measurement of partitioned axial displacements at both flanges

## EXPERIMENTAL RESULTS

### Crack patterns

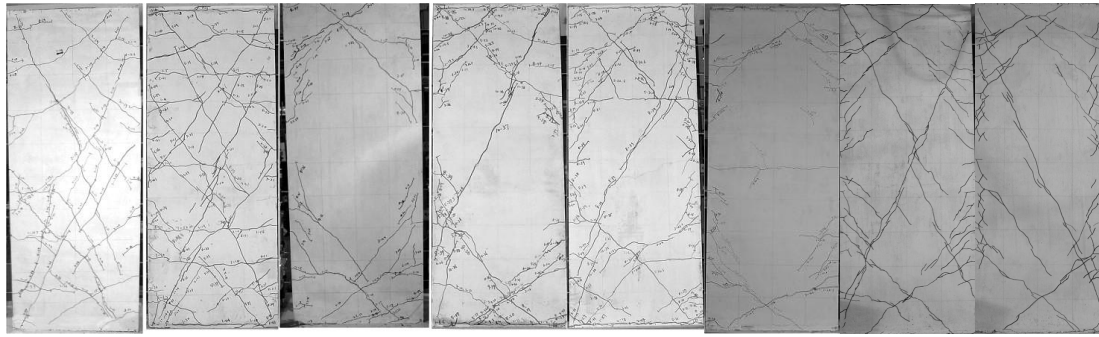
During the response in the  $R = 1/700$  cycle, bending cracks were observed for all specimens at beam-ends. In the  $R = 1/400$  cycle, bending-shear cracks were observed for the nominal series specimens. Diagonal shear cracks occurred at the center in the  $R = 1/100$  cycle except in specimens # N-3 and 6. For the specimens with de-bonded diagonal reinforcements (#N-3-8), cracks concentrated on both edge parts and the number of cracks was small. For the I-series specimens, a very small number of cracks concentrated on both edge parts with no shear crack at the center until large deformation occurred, except in #I-1. Crack patterns in the  $R = 1/100$  and final cycles are shown in Figures 7 and 8.

### Load-deflection curves

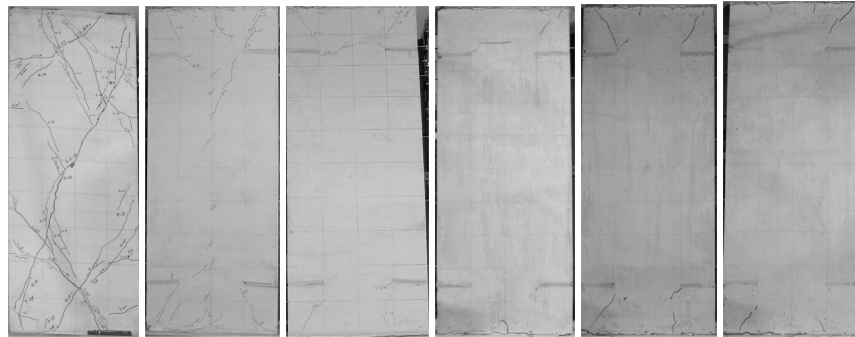
The load-deflection behavior of the specimens are shown in Figure 9. Significant differences were not observed between the hysteretic response of the specimens until the  $R = 1/40$  cycle for N-series specimens. During the response in the  $R = 1/40$  cycle, strength degradation was observed due to shear yield for specimen #N-1, of diagonal reinforcements buckling at the center in negative loading for specimen #N-2, of bond failure for specimen #N-3, and of diagonal shear slip at the end for specimen #N-4. No degradation was observed for specimens #N-5, 6, 7, and 8.

For I-series specimens, the load-deflection curves are fat, and energy dissipation ability is larger than in the N-series specimens, except in #I-1. Specimens #I-2, 4, and 5 have pinching phenomenon at the occurrence of large deformation after  $R = 1/67$ . This seems to be caused by the axial bars that work as bending bars. In the relation of #I-2 at the second  $R = 1/40$  cycle, the load dropped because one of the X bars fractured at the welded part. These bars of specimens #I-2 and 3 were quench-hardened for strengthening, and weldability was not good.





No. N-1    No. N-2    No. N-3    No. N-4    No. N-5    No. N-6    No. N-7    No. N-8

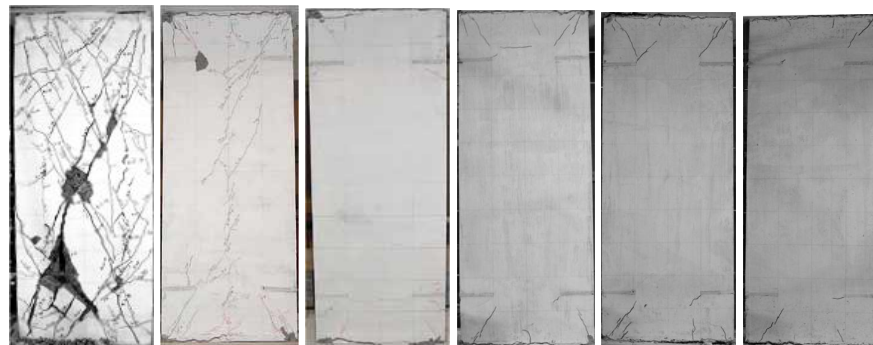


No. I-1    No. I-2    No. I-3    No. I-4    No. I-5    No. I-6

**Figure 7 : Crack Patterns ( $R=1/100$ )**



No. N-1    No. N-2    No. N-3    No. N-4    No. N-5    No. N-6    No. N-7    No. N-8



No. I-1    No. I-2    No. I-3    No. I-4    No. I-5    No. I-6

**Figure 8 : Crack Patterns (Final)**

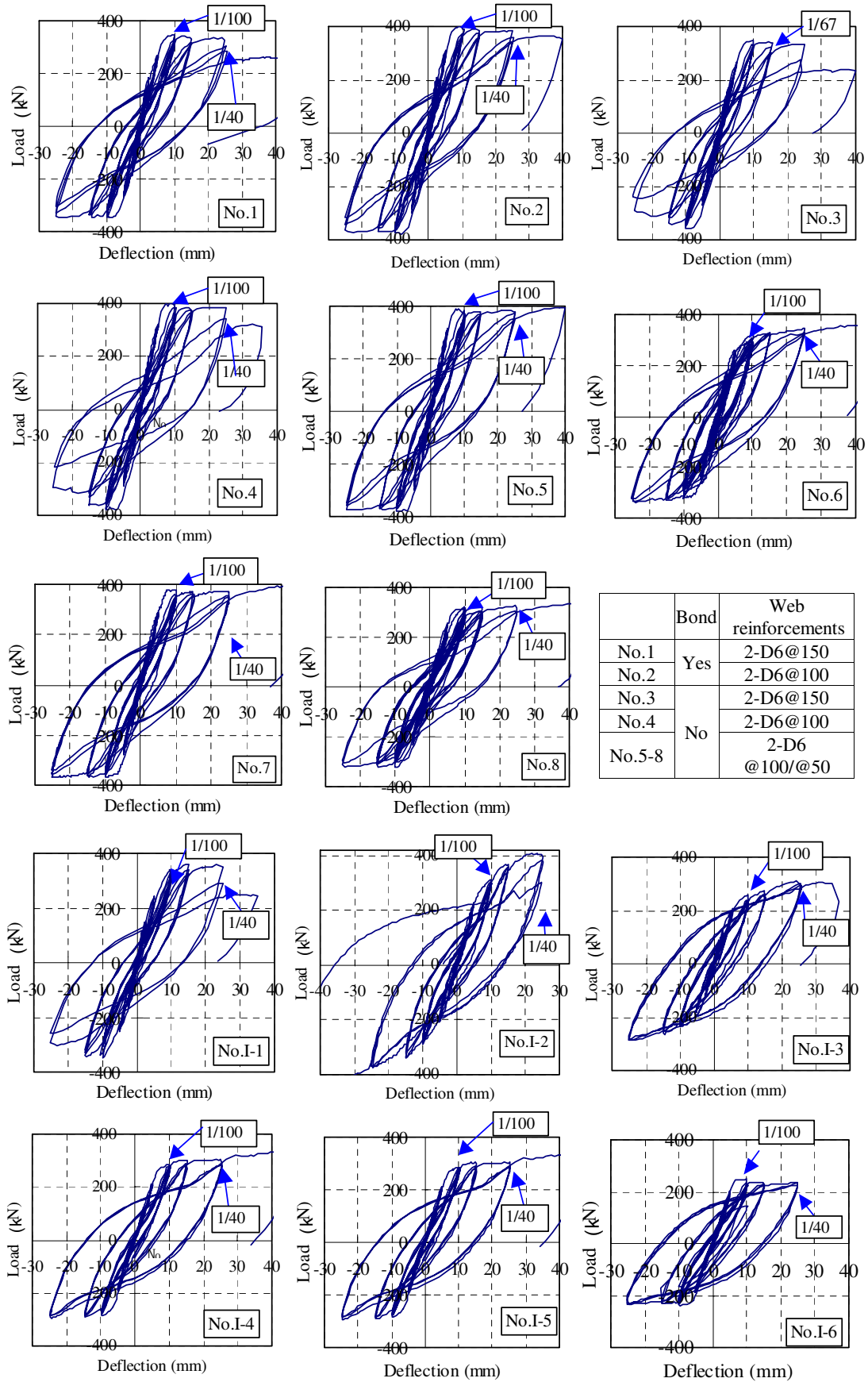


**Figure 9 : Load-Deflection Curves**

## INTERPRETATIONS OF TEST RESULTS

### Load-deflection relation

The force-displacement behavior can be predicted based on the assumption that the behavior is the sum of a parallel-reinforced R/C beam and diagonal steel braces as shown in Figure 10. For the R/C beam, flexural crack  $M_c$  and yield strength  $M_y$  are calculated by approximate Equations (1) and (2), and stiffness reduction factor  $\alpha_y$  (Secant modulus at yield point/initial stiffness) is obtained by experimental Equation (3) [4].

$$M_c = 0.56 \sqrt{\sigma_B} Z \quad (\text{units: N, mm}) \quad (1)$$

$$M_y = 0.9 a_t \sigma_y d \quad (2)$$

$$\alpha_y = (-0.0836 + 0.159 a/d)(d/D)^2 \quad (3)$$

where  $\sigma_B$  is concrete strength in  $\text{N/mm}^2$ ,  $Z$  is section modulus,  $a_t$  is area of longitudinal tension reinforcement,  $\sigma_y$  is yield strength of steel,  $d$  is distance from extreme compression fiber to centroid of tension reinforcement,  $D$  is height of beam, and  $a$  is shear span length ( $M/Q$ ). The diagonal reinforcements are assumed to be the bi-linear load-deflection relation and to act in both tension and compression.

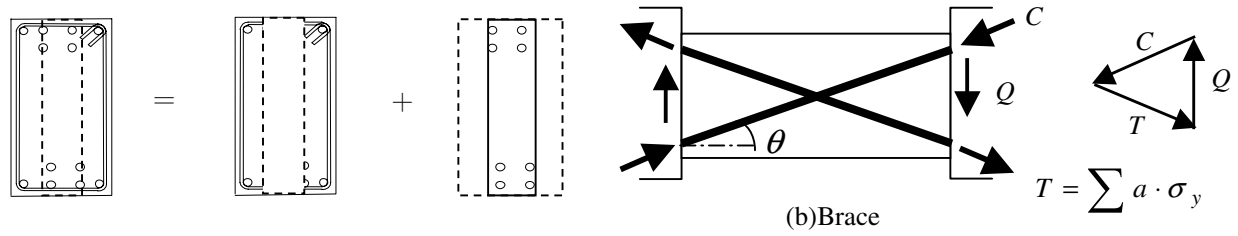


**Figure 10 : Load carrying model**

The envelope curves of the test results were compared with the calculated load-deflection relations in Figure 11. Both show good agreement for the N-series. For I-series specimens with axial rebars, resistance load increases with deformation and becomes larger than the calculated one. This is caused by the effect of axial rebars as bending reinforcements.

For design, this approximate calculation method can be employed to estimate the load-deflection behavior for diagonal reinforcement beams while fully satisfying the design.

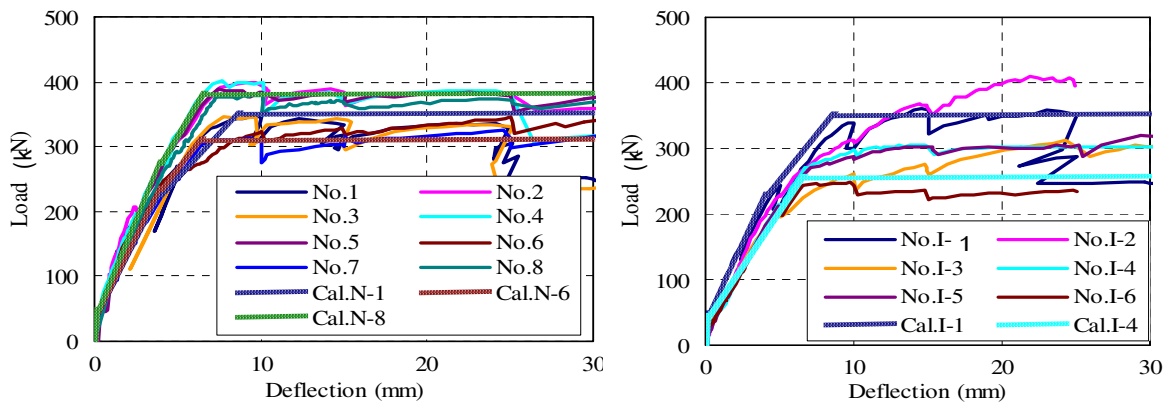


**Figure 11 : Load-Deflection Curves**



### Strain of reinforcements

Figure 12 shows the strain distribution of the diagonal reinforcements for specimens #N-1, 5 and 8 at the first peak load in each cycle. Strains of the de-bonded reinforcements (#N-5 and 8) are almost uniform in each cycle even on the compression side, in contrast with the bonded one (#N-1), in which the strain was influenced by the bending moment on the compression side. The reinforcements yielded during cycle  $R = 1/200$  to  $R = 1/100$  for all specimens. Compression strain of specimens #N-5 and 8 is small because the concrete struts act in compression.

For I-series specimens, compression strain is larger than that of N-series specimens, and tension strain becomes small. The notch method appears to work well.

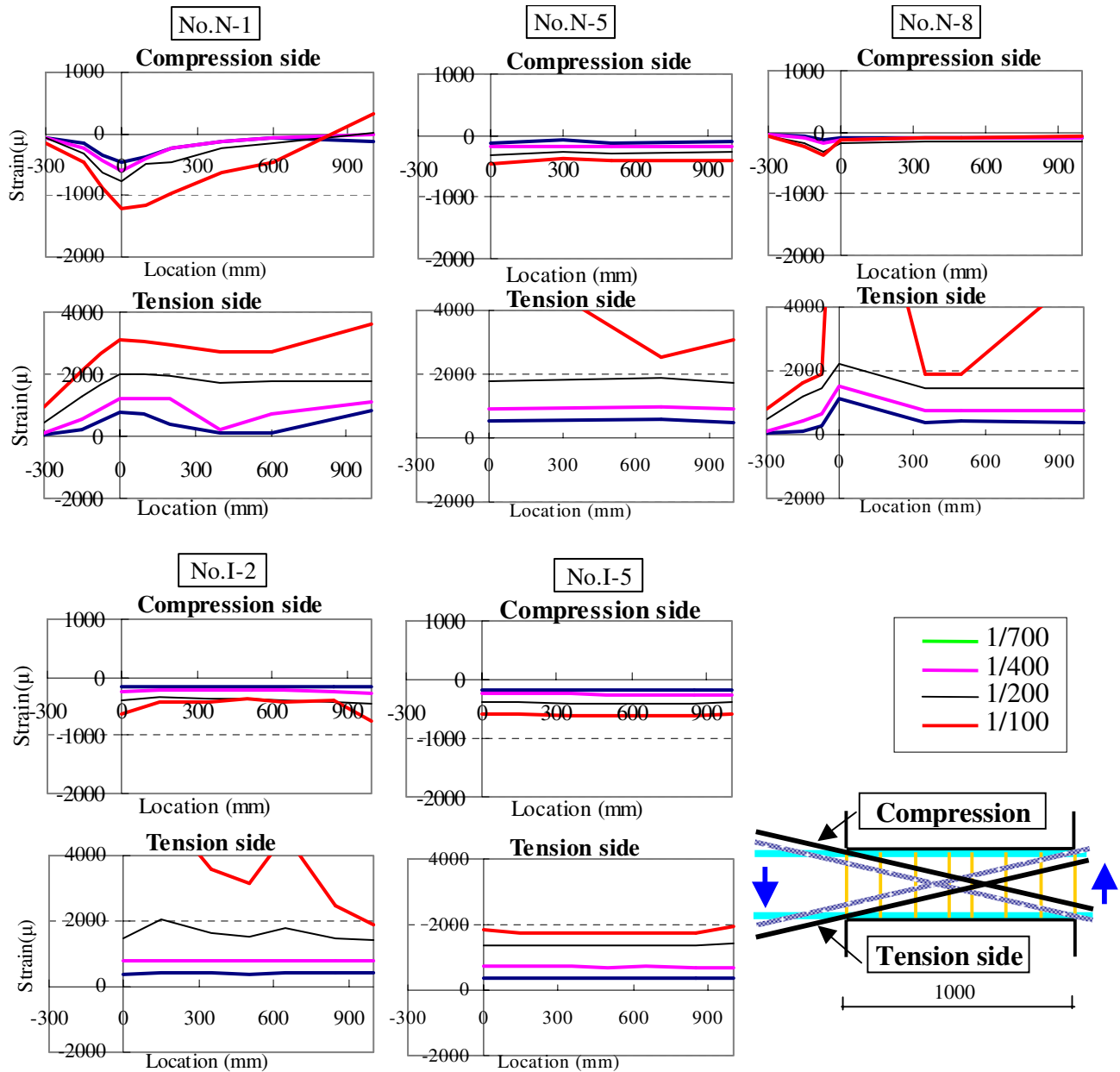


**Figure 12 :** Typical strain distribution of diagonal

Figure 13 shows the strain distribution of the parallel reinforcements at the first peak load in each cycle. During cycle  $R = 1/200$  to  $R = 1/100$ , the decline angle of strain distribution on the tension side is larger in specimens #N-5 and 8, which have de-bonded diagonal reinforcements, than in #N-1. This is caused by the difference of compression strain of the diagonal reinforcements shown in Figure 12. This means that the bond stress in specimens #N-3, 5, and 8 is larger than in #N-1 and it is a severe value for bond failure and shear stress based on truss mechanism. For this reason, additional web reinforcements are required at this region.

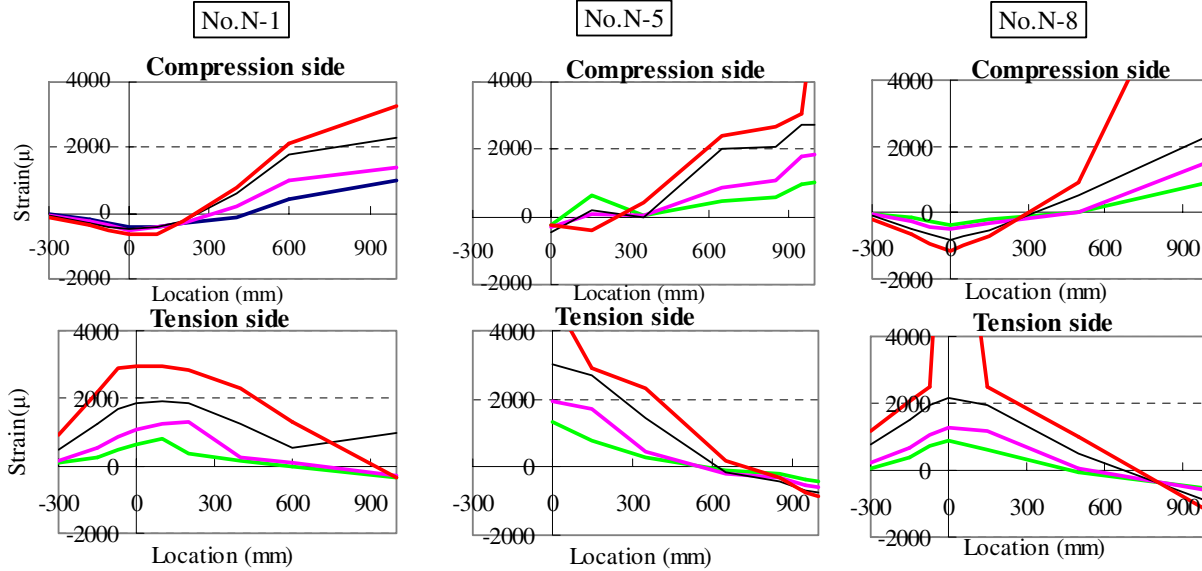


**Figure 13 :** Typical strain distribution of parallel reinforcements

### Bending and shear deformation

Bending deformation was calculated by integrating the curvature obtained from the piecewise axial displacement difference of both flanges. Shear deformation was calculated by subtracting the bending deformation from the total deformation.

Figure 14 shows the change of deformation components of bending deformation and shear deformation. The shear deformation part increases with increasing total deformation caused by shear cracks. Specimen #N-1 had large shear cracks in the center part, so the shear deformation part becomes much larger than that of the other specimens with slight cracking in the center. As specimen #N-6 had no shear cracks during the  $R = 1/100$  cycles, shear deformation is the smallest of the N-series specimens. The shear cracks at the end part for specimens #N-3, 6, 7 and 8 caused a bending hinge at both beam-ends. Specimens of I-series had no shear cracks even at the occurrence of large deformation, except #I-1, so that shear deformation is minimal.

### Axial elongation

Total axial elongation is defined as the elongation of the distance of both end stabs. Figure 15 shows the axial residual elongation at the end of each drift cycle. Until the  $R = 1/200$  cycle, the axial residual elongation was not measured. At the  $R = 1/100$  cycle, the axial elongation increases for all specimens due to yielding of the diagonal and longitudinal reinforcements. The elongation is larger in specimens #N-3, 5, 7, and 8 than that in specimen #N-1 during the  $R = 1/100$  and  $1/67$  cycles. This difference is caused by the compression strain of the diagonal reinforcements shown in Figure 12. The compression strain of bonded diagonal reinforcement becomes large, because the concrete is compressed by bending, and this

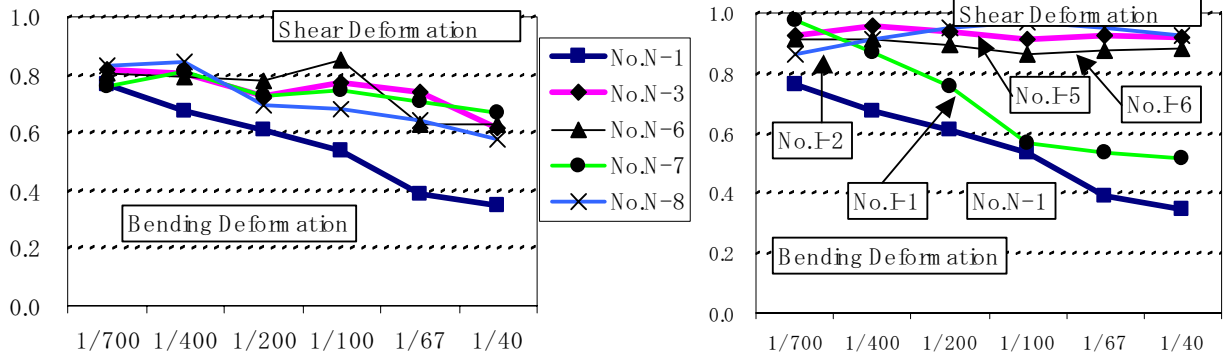


**Figure 14 : Changing of deformation component**

compression stress is propagated to the diagonal bar by bond stress. The de-bonded diagonal reinforcements are not influenced by the concrete compression stress, and act only as a compression brace. However, a concrete arch strut acts with them, so the compression stress of the de-bonded diagonal reinforcements is small. As accumulated tension stress increased in the de-bonded diagonal reinforcements, the axial elongation in specimens #N-3, 5, 7 and 8 became large.

The axial elongation in specimen #I-3 is almost the same as in specimen #N-1; however, it seems to be rather small. This difference is caused by the compression strain of the diagonal reinforcements as a result of the notch working effectively. The axial elongation in specimens #I-2 and 5 with axial reinforcements is smaller than that in specimen #I-3. The axial reinforcements worked effectively.

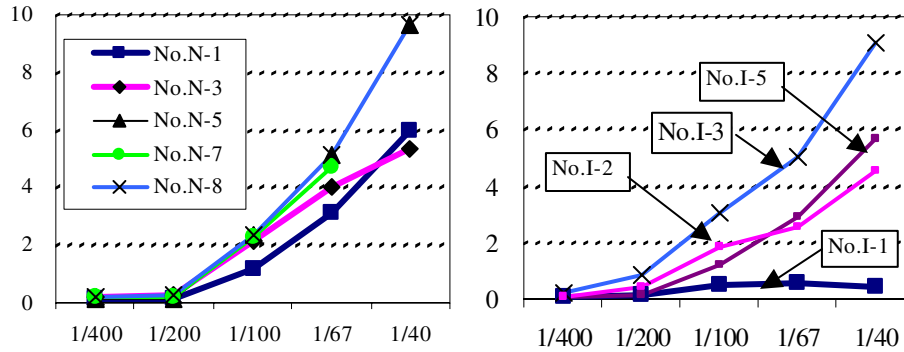


**Figure 15 : Relation of axial elongation versus drift**

### Equivalent damping factor

Figure 16 shows the equivalent damping factor of each specimen calculated from the first half cycle of the applied load – total deflection relationship shown in Figure 9. Significant differences were not observed in the equivalent damping factor between all N-series specimens. This means that the energy dissipation ability is the same, despite the clear difference of crack patterns shown in Figures 7 and 8 caused by the presence or absence of bond of the diagonal reinforcements.

For I-series specimens, the equivalent damping factor becomes large compared with the N-series' value after the  $R = 1/100$  cycle. For the #I-2 specimen, the value was reduced because bond cracks of the axial reinforcements developed and stiffness degrading near zero load occurred as shown in Figure 9.

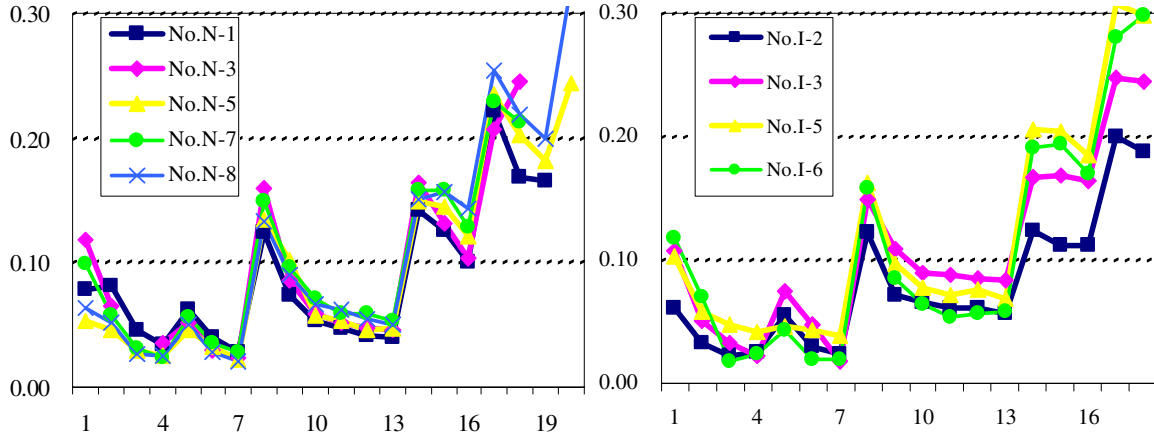


**Figure 16 : Fluctuations in equivalent damping factor**

### Macro model and damage evaluation

To evaluate the load resisting system and the condition of whether or not shear cracks developed at the central part, the load-carrying model shown in Figure 10 was modified as shown in Figure 17. A beam is divided into two systems, one diagonal steel bar truss system with concrete strut and the other a parallel-reinforced beam. In the diagonal truss system, tension force is only by steel bars ( $T_s$ ), and compression force is a combination of steel bars ( $C_s$ ) and concrete strut ( $C_c$ ). As the tension force and the compression force should be equal for both the diagonal truss system and the parallel beam system, the compression force of concrete struts can be evaluated from the difference of force of the diagonal steel bar estimated from strain gage data. The ratio of  $C_s/T_s$  is shown in Figure 18(a)(b) for specimens #N-5, 6, 7 and 8 at the  $R = 1/400$  and  $1/200$  cycles. These values are almost constant despite the difference of concrete strength or yield strength of the steel bars. It is about 0.15 for the X brace system and 0.35 for the parallel beam system.

For the parallel reinforcement beam, the compression stress of concrete was calculated by elastic beam theory using steel bar force ( $T_s$ ) estimated from strain data. The area of compression was assumed from extreme compression fiber to neutral axis calculated from strain data of steel bars. According to the elastic beam theory, there is no compression stress of concrete in the middle part of the beam. Figure 18(c) shows the depth of compression area for specimens #N-5, 6, 7 and 8 at the  $R = 1/400$  and  $1/200$  cycles. In this figure, the calculated values using the elastic beam theory for the parallel beam section shown in Figure 10(a) are also plotted. These values are also almost constant, and are about 0.2 times the total depth. This compression area is used for the brace system to obtain the compression stress of concrete struts.

Shear force for concrete was calculated by subtracting the vertical force of the diagonal steel bar ( $T_s + C_s$  in Figure 17(a)) from the total shear force. Maximum shear stress of concrete is calculated as 1.5 times the mean shear stress for the all-rectangular section.

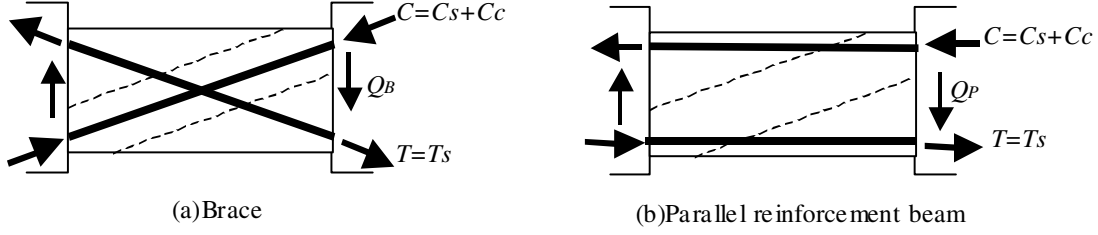


**Figure 17 : Macro model**

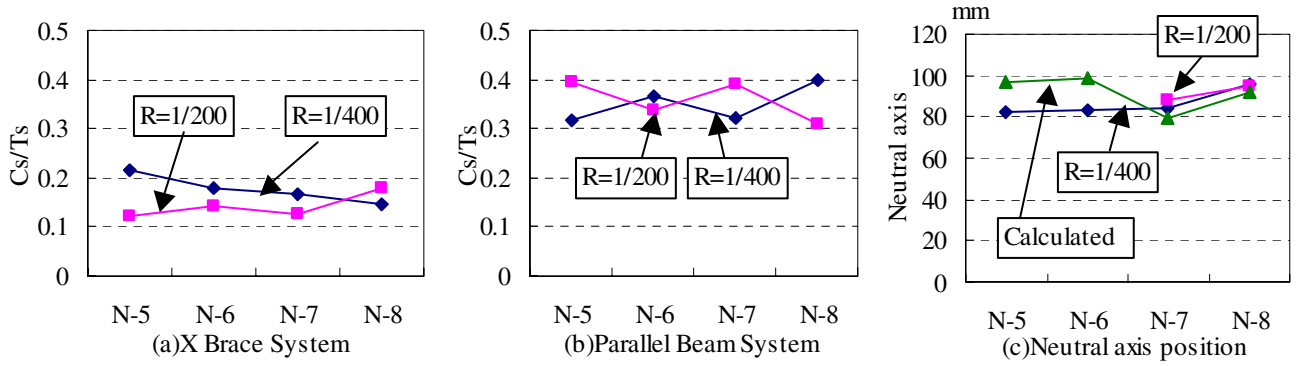


**Figure 18 : Ratio of compression force to tension force of steel bar**

Using horizontal component of compression stress, tension stress by Poisson's effect ( $\nu = 1/6$ ), and shear stress, the principal tension stress is calculated by Mohr's circle. Figure 19 shows the calculated results at the calculated maximum load as the ratio to the square root of concrete strength in Figure 19(a), and to the concrete strength in Figure 19(b). Shear stress is also plotted in the same figure. The principal stress and the shear stress are almost the same. The specimens having large tension stress had the diagonal shear crack at an early load cycle. It seems that this model shows good agreement for examining the load-carrying system. I-series specimens have no compression concrete strut because of the notch. Therefore, as steel bars carry almost all of the shear force, the tension stress of concrete becomes nearly zero. The test results showed no diagonal shear crack.

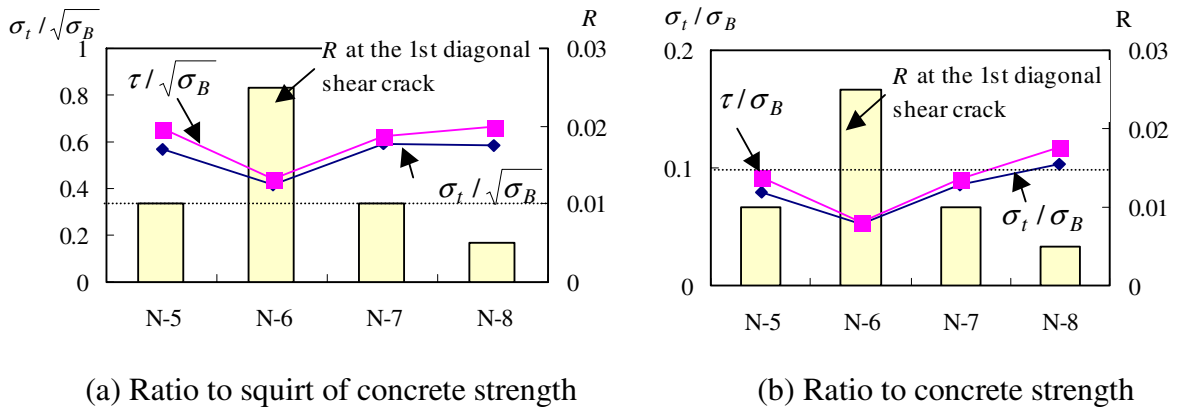


**Figure 19 : Ratio of tension stress**



## CONCLUSIONS

This paper examined the behavior of short beams with diagonal reinforcements to reduce damage during a severe earthquake for good repairability. The main findings are as follows:

1. The results of this experimental investigation demonstrated that de-bonded diagonal reinforcements are an effective means to reduce the number of cracks for short beams.
2. Significant differences were not observed between the hysteretic response and equivalent damping factor of the specimens. The equivalent damping factor of the I-series specimens is larger than that of the N-series.
3. The approximate calculation method (sum of a parallel reinforced R/C beam and diagonal steel braces) can be employed to estimate the load-deflection behavior for diagonal reinforcement beams while fully satisfying the design.
4. Strains of the de-bonded diagonal reinforcements are almost uniform in each cycle and free from bending stress.
5. The axial elongation is larger in the de-bonded specimens than in the bonded specimens. This can reduce the use of axial reinforcements.
6. The macro model showed good agreement with the tested results.

This is a continuing project, and more detailed load resistance systems will be analytically investigated.

## ACKNOWLEDGEMENT

This study was carried out as part of the TEDCOM (Typhoon and Earthquake induced Disaster Control and Mitigation) project in Kanagawa University, funded by the Ministry of Education, Culture, Sports, Science and Technology (Frontier Research Program) and Yokohama city (collaboration program between industry, academia, and the government). The opinions and findings do not necessarily represent those of the sponsor.

## REFERENCES

1. Park, R. and T. Paulay, Reinforced Concrete Structures, A WILEY-INTERSCIENCE PUBLICATION, 1975
2. Eto, H., K. Yoshioka, et al., Aseismic design of 41 story reinforced concrete tube structure –Part 4 Ultimate shear strength of short beams–, Summaries of technical papers of annual meeting, C, Architectural Institute of Japan, 1989, pp.773-774 (In Japanese)
3. Shimazaki, K. and Y. Hayakawa, Experimental study for ductility of short beams, Proceedings of the Japan Concrete Institute, 1990, pp.179-184 (In Japanese)
4. AIJ, AIJ Standard for structural Calculation of Reinforced concrete Structures –Based on Allowable Stress Concept–, Architectural Institute of Japan, 1999.
5. AIJ, Design Guidelines for Earthquake Resistant Reinforced Concrete Buildings Based on Inelastic Displacement Concept, Architectural Institute of Japan, 1999.